Mason, H. E., Yates, J. L. R., Potts, R. J., Gutmann, M. J., Howard, J. A. K., & Sparkes, H. A. (2021). Structural studies of N-(methoxysalicylidene)-fluroaniline, N-(methoxysalicylidene)-chloroaniline and N-(methoxysalicylidene)-bromoaniline derivatives. *Acta Crystallographica Section B: Structural Science, Crystal Engineering and Materials*, *B77*(6), 974-980. https://doi.org/10.1107/S2052520621009835

Peer reviewed version

Link to published version (if available):
10.1107/S2052520621009835

Structural studies of *N*-(methoxysalicylidene)-fluroaniline, *N*-(methoxysalicylidene)-chloroaniline and *N*-(methoxysalicylidene)-bromoaniline derivatives

Authors

Helen E. Mason[a1], Jane L. R. Yates[a], Rachael J. Potts[b], Matthias J. Gutmann[c], Judith A. K. Howard[a] and Hazel A. Sparkes[b]*

[a]Durham University, Department of Chemistry, University Science Site, South Road, Durham, DH1 3LE, United Kingdom

[b]University of Bristol, School of Chemistry, Cantock's Close, Bristol, BS8 1TS, United Kingdom

[c] ISIS Facility, STFC-Rutherford Appleton Laboratory, Didcot, OX11 OQX

Correspondence email: hazel.sparkes@bristol.ac.uk

[1]Died December 2019.

Synopsis Structural studies into twenty-seven *N*-(methoxysalicylidene)-haloaniline (halo = F, Cl or Br) compounds. New polymorphs were identified for two of the compounds and a phase transition was also identified for another. The link between their structures and visual observations of their thermochromic behaviour are made.

Abstract Twenty-seven *N*-(methoxysalicylidene)-haloaniline (halo = F, Cl or Br) compounds were synthesised. The crystal structures of all twenty-seven compounds have been determined at low temperature and are reported herein, along with a variable temperature neutron diffraction study on two of the compounds. New polymorphs were identified for two of the compounds along with a temperature induced phase transition for one of the other compounds. Visual observations on the thermochromism of the 27 compounds are also reported. The *inter*planar angle between the two aromatic rings and the *inter*molecular interactions in the structures are examined and linked to the visual observations on the thermochromism.

Keywords: Schiff bases; thermochromism; polymorphism

1. Introduction

The relatively easy synthesis of a wide range of Schiff bases makes them versatile ligands and consequently they have found widespread use in many areas including organometallic chemistry (Kargar *et. al.*, 2020), polymer synthesis (Mighani, 2020), anticancer drugs (Parveen, 2020), catalysts

(Kumari *et. al.*, 2019) and sensors (Sahu *et. al.*, 2020). In addition, Schiff bases themselves have been found to display interesting properties with anils, Schiff bases of salicylaldehyde derivatives with aniline derivatives, having been found to exhibit both thermo- and photochromism in the solid-state (Senier *et. al.*, 1909; Cohen *et. al.*, 1962; Cohen *et. al.*, 1964). Originally the thermo and photo chromism of anils were thought to be mutually exclusive (Cohen *et. al.*, 1962; Cohen *et. al.*, 1964) but this has since been found not to be the case and it is thought they all display thermochromism with some also displaying photochromism (Fujiwara *et. al.*, 2004). The colour change was initially attributed to a light or thermally induced tautomeric equilibrium shift between colourless enol(-imine) and coloured keto(-amine) forms (Hadjoudis *et. al.*, 2004; Robert *et. al.*, 2009), see Figure 1. In both cases the chromism involves an intramolecular proton shift from the *ortho*-hydroxy group, crucial for the mechanism to occur, to the imine nitrogen atom. Evidence for the thermochromic mechanism was first observed in *N*-(5-chlorosalicylidene)-4-hydroxyaniline with the population of the *cis*-keto form increasing with decreasing temperature, with the ratio of OH to NH forms changing from 31:69 at 299 K to 10:90 at 90 K (Ogawa *et. al.*, 1998) and at 15K it is believed to be solely the NH form (Ogawa *et. al.*, 2000). The photochromic mechanism has been observed in single crystals of *N*-3,5-di-*tert*-butylsalicylidene-3-nitroaniline (Harada *et. al.*, 1999). After 4 hours irradiation at room temperature, using 2-photon excitation at 730 nm, the structure of the dark-red photo product at 90 K was found to contain both the enol and *trans*-keto form at a ratio of 90:10. Irradiation at room temperature using light with $\lambda > 530$ nm caused the crystal to return to the pale yellow colour of the enol form and demonstrated the reversibility of the mechanism.

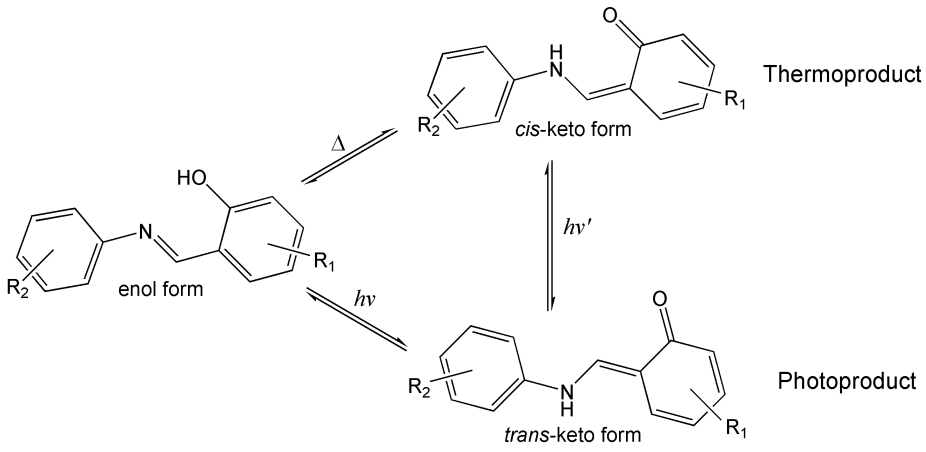

Figure 1 Illustration of the enol to keto tautomerism mechanism which affects that colour change in anils.

The enol to keto tautomerism isn't the whole picture, Harada *et al.* identified that thermochromism in anils can only be explained by taking into account the fluorescence and not just the tautomeric equilibrium between enol and *cis*-keto forms (Harada *et. al.*, 2007). The impact of the fluorescence becomes particularly significant for thermochromic compounds at lower temperatures and can in fact

dominate as the cause of the thermochromic colour change. While at higher temperatures the keto-enol tautomerism is dominant for thermochromic compounds.

The synthesis of twenty-seven *N*-(methoxysalicylidene)-haloaniline (halo = F, Cl or Br) compounds are reported. The crystal structures of all of the compounds are reported at low temperature. Ten of the structures had previously been reported at room temperature, however they are reported herein at low temperature for completeness. For two other compounds new polymorphs were identified herein while a further compound was found to undergo a temperature induced phase transition. Visual observations were made of the thermochromic colour change upon cooling for all of the compounds. These were linked to the structural properties of the various compounds.

Table 1 Studied compounds and their reference numbers

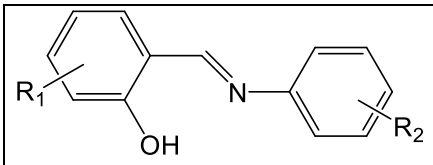

R_1 = OMe
R_2 = Br, Cl, F

Compound reference number	Substituents
1-F	R_1 = 3-OMe, R_2 = 2-F
2-F	R_1 = 4-OMe, R_2 = 2-F
3-F	R_1 = 5-OMe, R_2 = 2-F
4-F	R_1 = 3-OMe, R_2 = 3-F
5-F	R_1 = 4-OMe, R_2 = 3-F
6-F	R_1 = 5-OMe, R_2 = 3-F
7-F	R_1 = 3-OMe, R_2 = 4-F
8-F	R_1 = 4-OMe, R_2 = 4-F
9-F	R_1 = 5-OMe, R_2 = 4-F
1-Cl	R_1 = 3-OMe, R_2 = 2-Cl
2-Cl	R_1 = 4-OMe, R_2 = 2-Cl
3-Cl	R_1 = 5-OMe, R_2 = 2-Cl
4-Cl	R_1 = 3-OMe, R_2 = 3-Cl
5-Cl	R_1 = 4-OMe, R_2 = 3-Cl
6-Cl	R_1 = 5-OMe, R_2 = 3-Cl
7-Cl	R_1 = 3-OMe, R_2 = 4-Cl
8-Cl	R_1 = 4-OMe, R_2 = 4-Cl
9-Cl	R_1 = 5-OMe, R_2 = 4-Cl
1-Br	R_1 = 3-OMe, R_2 = 2-Br
2-Br	R_1 = 4-OMe, R_2 = 2-Br
3-Br	R_1 = 5-OMe, R_2 = 2-Br
4-Br	R_1 = 3-OMe, R_2 = 3-Br
5-Br	R_1 = 4-OMe, R_2 = 3-Br
6-Br	R_1 = 5-OMe, R_2 = 3-Br
7-Br	R_1 = 3-OMe, R_2 = 4-Br
8-Br	R_1 = 4-OMe, R_2 = 4-Br
9-Br	R_1 = 5-OMe, R_2 = 4-Br

2. Experimental

2.1. Reagents and techniques

All reagents were used as supplied from Aldrich. Compounds were synthesized by direct condensation of the appropriate salicylaldehyde and aniline derivatives in ethanol. 0.0025 moles of the salicylaldehyde and aniline were each dissolved in 25 ml of ethanol, the resulting solutions combined and refluxed with stirring for four hours. Any precipitate was filtered off rinsed with ethanol and left to dry, the (remaining) solution was then rotary evaporated until (further) precipitate formed. Re-crystallization was carried out from ethanol and acetonitrile for all compounds. The compounds synthesised along with the reference numbers used to refer to them throughout this paper are listed in Table 1.

2.2. Crystallographic data collection

Single crystal X-ray diffraction measurements for **1-F** to **9-F**, **7-Cl** to **9-Cl** and **1-Br** to **9-Br** were collected at 120(2) K, **9-Br** was also collected at 220(2) K on Bruker Smart 1K diffractometer, **1-Cl** to **3-Cl** were collected at 120(2) K, **4-Cl** and **6-Cl** were collected at 100(2) K and **5-Cl** was collected at 150(2) K on a Bruker ApexII diffractometer. All datasets were collected using graphite monochromated Mo Kα radiation (λ = 0.71073 Å) and recorded on a CCD detector. Cells were also checked at 300(2) K for all structures. Structures **1-F** to **9-F**, **7-Cl** to **9-Cl** and **1-Br** to **9-Br** were solved using direct methods in ShelXS (Sheldrick, 2008) and **1-Cl** to **6-Cl** were solved using Superflip (Palatinus *et. al.*, 2007; Palatinus *et. al.*, 2008; Palatinus *et. al.*, 2012). All structures were refined by full matrix least squares on F^2 using SHELXL (Sheldrick, 2008; Sheldrick, 2015) in Olex2 (Dolomanov *et. al.*, 2009). All hydrogen atoms, apart from the OH hydrogen involved in the intramolecular hydrogen bonding with the imine nitrogen atom were positioned geometrically (aromatic and C8-H8 C-H 0.95 Å, methyl C-H 0.98 Å) and refined using a riding model. The isotropic displacement parameter of the hydrogen atom was fixed at U_{iso}(H) = 1.2 times U_{eq} of the parent carbon atom for the aromatic hydrogen atoms and C8-H8, while U_{iso}(H) = 1.5 times U_{eq} for the parent carbon atom for the methyl hydrogens. The hydrogen atoms involved in the intramolecular hydrogen bond were located in the Fourier difference map (FDM) wherever feasible or fixed geometrically (O-H 0.84 Å, U_{iso}(H) = 1.2 times U_{eq} of the parent oxygen atom) for **6-F**, **5-Br** and **6-Br** where this was not possible. Crystal packing diagrams were created and analyzed using Mercury (Macrae *et. al.*, 2008). The *inter*planar dihedral angle was calculated by measuring the angle between planes computed through the six carbon atoms of the two aromatic rings. See ESI Tables S1-S3 in the supplementary information for further details of the crystallographic data collections.

Single crystal neutron diffraction data for **3-Cl** and **3-Br** were collected at 120 and 300 K on SXD at ISIS (Keen *et. al.*, 2006), by mounting a single crystal on a closed cycle refrigerator and using 4-5 crystal settings. Data were processed using SXD2001 (Gutmann, 2005).

2.3. Diffuse reflectance spectroscopy

Diffuse reflectance spectra were measured for **1-Br** to **9-Br**. The sample was ground to give uniform particle distribution and placed in a 40 x 10 x 2 mm quartz cuvette to ensure optical thickness. A cuvette sample holder with a white polytetrafluoroethylene (PTFE) block spacer was used to load the sample into an Oxford Instruments Cryostat. The sample was irradiated with an Ocean Optics halogen light source and an Avantes AvaSpec-2048-2 CCD detector (placed at an acute angle to minimize detection of specular reflectance) collected the reflectance spectra which were recorded using AvaSoft basic software. Cryostat temperature control was performed using an Oxford Intelligent Temperature Controller, each temperature was stabilized for 10 min or until ±0.1 K before recording the spectrum. A white PTFE block was used to record a reference spectrum before each data set collection. The diffuse reflectance spectra are illustrated as % reflectance versus wavelength and Kubelka-Munk function, *F(R)*, versus wavelength. If *S* is independent of λ, then *F(R)* versus λ is equivalent to the absorption spectrum for a diffuse reflector. To allow basic trends to be easily observed moving averages were applied to data during analysis.

3. Results and discussion

3.1. Crystal Structures

The crystal structures of compounds **1-F** (Unver *et. al.*, 2002), **1-Cl** (Francis *et. al.*, 2003), **2-Cl** (Kosar *et. al.*, 2009), **3-Cl** (Ozek *et. al.*, 2008a), **6-Cl** (Ozek *et. al.*, 2008b), **8-Cl** (Kosar *et. al.*, 2009), **9-Cl** (Ozek *et. al.*, 2008c), **3-Br** (Ozek *et. al.*, 2007), **6-Br** (Ozek *et. al.*, 2007) and **7-Br** (Zheng *et. al.*, 2005) have previously been reported. The structures obtained herein were consistent with the previously published structures. Different polymorphs, to those previously published, were obtained in this study for **8-F** (Albayrak *et. al.*, 2010) and **7-Cl** (Yeap *et. al.*, 2003) and a phase transition upon cooling was observed for **9-Br** (Ozek *et. al.*, 2007). The structures reported herein will be denoted as **8-F(2)**, **7-Cl(2)** and **9-Br(LT)**. The structures of the remaining compounds are included here at low temperature for completeness as the published structures are at room temperature. They also demonstrate that for the majority of them no structural changes are observed upon cooling.

The 27 compounds all crystallised with one molecule in the asymmetric unit (*Z*'=1) with the exception of **7-Cl(2)** which contained two unique molecules in the asymmetric unit (*Z*'=2) in this study. However, the previously published polymorph of **7-Cl(1)** had one molecule in the asymmetric unit (*Z*'=1) (Yeap *et. al.*, 2003). The basic structure of the 27 compounds is the same containing a methoxy substituted hydroxy-phenyl group and a halogen substituted phenyl group joined by an imine group (Figure 2). The imine group C8=N1 bond lengths range from 1.263(12) in **6-Br** to 1.299(10) in **9-Br(LT)**, while the hydroxyl-phenyl C2-O2 bond lengths range from 1.343(4) in **8-Cl** to 1.364(7) in **5-Br**. These C8=N1 and C2-O2 are consistent with the bonds being double and single bonds respectively (Allen *et. al.*, 1987), indicating that the crystal structures are all in the enol form. An

*intra*molecular hydrogen bond creates a quasi-six-membered ring O2-H2···N1-C8-C7-C2, which shows only small deviations from planarity (maximum 0.0293 Å for **2-F**, calculated as deviations from the plane through the five non-hydrogen atoms, this value was less for the other compounds).

Examining the intermolecular interactions in the structures showed the presence of C-H···O (Gu *et. al.*, 1999), and also in the case of **1-F** to **9-F** C-H···F (D'Oria *et. al.*, 2008; Thalladi *et. al.*, 1998), interactions in all of the structures. In addition, a small number of the structures also contained π-π interactions (ESI Tables S4-S8). The C-H···O interactions involve the methoxy oxygen (O1) and/or hydroxy oxygen (O2) atoms interacting mainly with aromatic C-H, although in the case of **5-F**, **8-F(2)**, **5-Cl** and **8-Br** only methyl C-H are involved (ESI Tables S4-S6). The C-H···F interactions also mainly involve aromatic hydrogen atoms, except **9-F** which also involved a methyl hydrogen atom and **6-F** which contains either short aromatic or methyl C-H···F interactions due to the disorder in the fluorine atoms (ESI Table S7).

3.2. Polymorph 8-F(2)

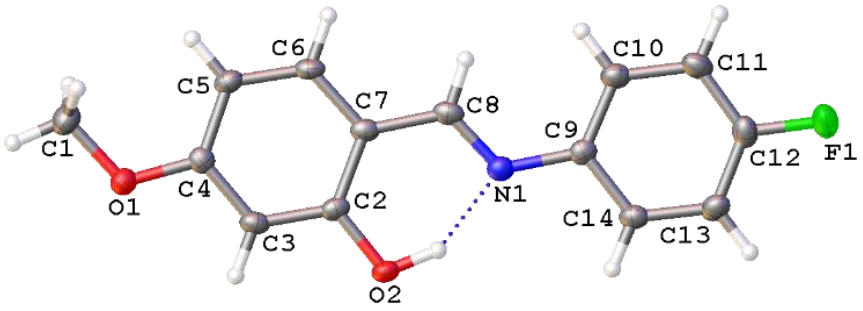

Figure 2 Structure of **8-F(2)** at 120(2) K with atomic numbering scheme depicted. Intramolecular hydrogen bond shown with dashed line.

The structure of **8-F** obtained in the current study, **8-F(2)**, see Figure 2, differs significantly from the previously published structure, denoted **8-F(1)** (Albayrak *et. al.*, 2010). Both polymorphs crystallised in the monoclinic crystal system, with **8-F(1)** in the space group *Pc* while **8-F(2)** was in the space group $P2_1/c$. However, there are key differences in the molecular conformations of the two polymorphs. Firstly while both polymorphs have the methyl group of the -OMe group in approximately the same plane as the phenyl group to which it is attached, for **8-F(1)** it is on the same side as the OH group while for **8-F(2)** it is on the opposite side to the OH group. Secondly, the two phenyl rings are orientated differently with respect to each, in **8-F(1)** the dihedral angle between the two phenyl rings is 48.17(1)° while for **8-F(2)** it is 2.07(9)° see Figure 3.

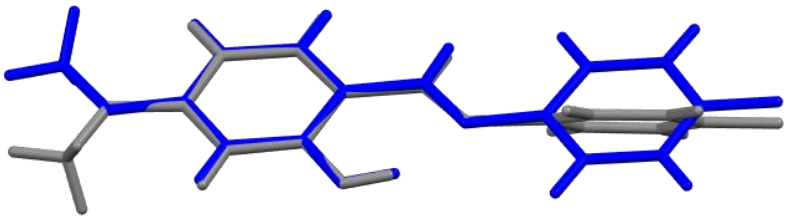

Figure 3 Overlay of molecule of (grey) **8-F(1)** at room temperature (blue) **8-F(2)** at 120(2) K.

The packing and intermolecular interactions for the two polymorphs are also quite different. In the case of **8-F(1)** all of the molecules are orientated in the same direction, and the structure shows C-H···F interactions between the methyl group and the fluorine atom of adjacent molecules. While in the case of **8-F(2)**, C-H···F interactions exist between an aromatic H adjacent to the F on one molecule and the F on an adjacent molecule. The structure also contains π-π interactions between adjacent molecules forming a stack in approximate the *a* axis direction.

3.3. Polymorph 7-Cl(2)

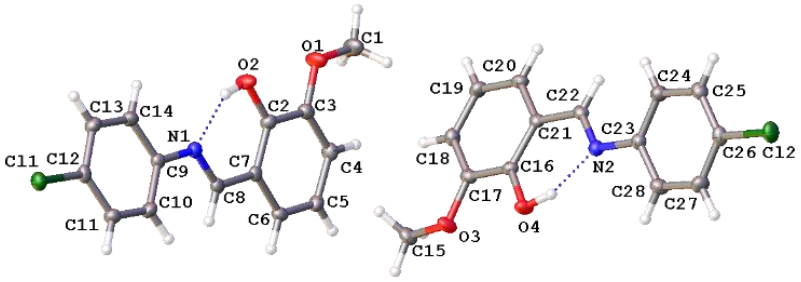

Figure 4 Structure of **7-Cl(2)** at 120(2) K with atomic numbering scheme shown. Intramolecular hydrogen bonding shown with dashed lines.

In the case of **7-Cl**, the previously published structure (**7-Cl(1)**) (Yeap *et. al.*, 2003) was obtained in the orthorhombic space group $P2_12_12_1$ with one molecule in the asymmetric unit. The dihedral angle between the two rings was ~11.9°. The structure of **7-Cl(2)** obtained herein crystallised in the monoclinic space group $P2_1/c$ with two molecules in the asymmetric unit, see Figure 4. The dihedral angles between the two phenyl rings were 11.75(11)° and 16.73(11)° for the two independent molecules, very similar to that seen for **7-Cl(1)**. The structure of **7-Cl(2)**, unlike **7-Cl(1)**, contains Cl···Cl interactions with Cl···Cl distances of 3.3618(7) Å and 3.3845(7) Å. Examining the packing of the two polymorphs shows that **7-Cl(1)** forms a herring bone type motif. While **7-Cl(2)** has a herring bone type motif in the *ab* plane, however it is two molecules wide in the *c*-axis direction and then as a result of the *c*-glide the zig-zag is the opposite direction still in the *ab* plane, see Figure 5.

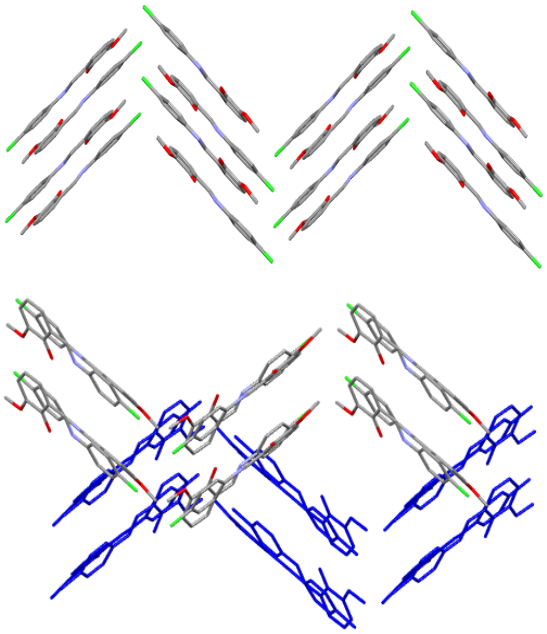

Figure 5 Packing for (top) **7-Cl(1)**, (bottom) **7-Cl(2)** with front pair of molecules in elemental colours and next pair behind in blue to show opposite zig-zag direction.

3.4. Temperature induced phase transition 9-Br

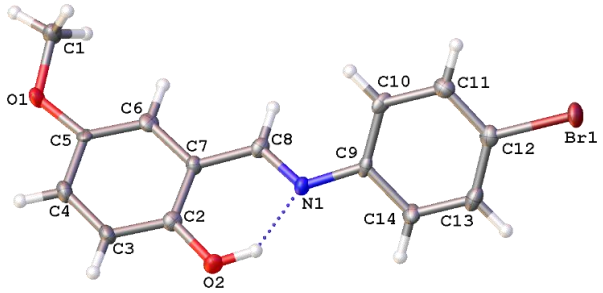

Figure 6 Structure of **9-Br** at 120(2) K with atomic numbering scheme shown. Intramolecular hydrogen bond shown with dashed line.

The structure of **9-Br** (Ozek *et. al.*, 2007) has previously been published at room temperature in the monoclinic space group *Pc*, see Figure 6. The structures obtained herein at 300(2) K and 220(2) K were consistent with the previously published structure. However, the structure was found to undergo a thermal phase transition upon cooling with no significant loss of crystallinity. At 120(2) K the structure was found to be in the monoclinic spacegroup *Cc*, with an approximate doubling of the *a* - axis length from 14.112(3) Å at 300(2) K to 27.874(5) Å at 120(2) K and a reduction in the β angle from 98.326(4)° at 300(2) K to 95.091(4)° at 120(2) K. The orientation of the molecule did not

change significantly as a result of the phase transition, see Figure 7, and the packing in both cases was almost identical.

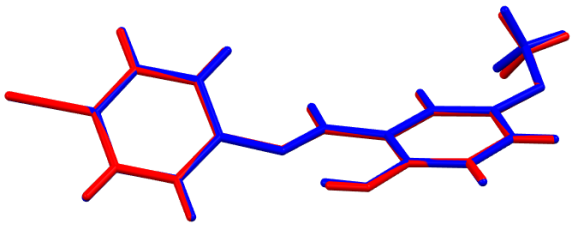

Figure 7 Overlay of one molecule of **9-Br** at (red) 300(2) K and blue 120(2) K.

3.5. Thermochromic observations

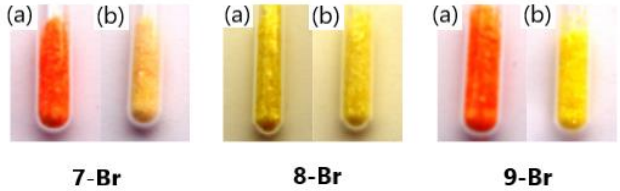

Figure 8 Microcrystalline powders of (left) **7-Br**, (middle) **8-Br** and (right) **9-Br** at (a) room temperature (b) after dipping in liquid nitrogen.

The anils are known to display thermochromism. Here all of the 3- or 5-methoxysalicylaldimine derivatives were found to be orange/red at room temperature and showed a reversible colour change to yellow when dipped in liquid nitrogen temperature (~77 K). The 4-methoxysalicyaldimine derivatives appear yellow at room temperature and show little or no colour change to the naked eye with decreasing temperature (see Figure 8 for a representative example). The colour change for the strongly thermochromic compounds can also be followed clearly by eye as a function of temperature, see Figure 9.

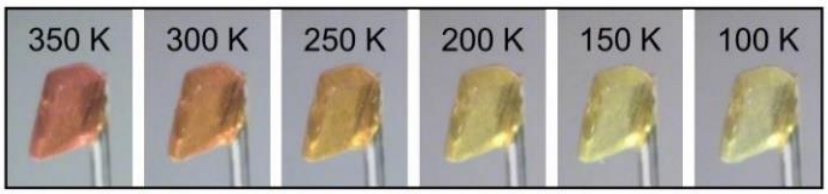

Figure 9 Illustration of the colour change upon cooling for **4-F**.

The thermochromic colour change was initially believed to be due solely to an enol to cis-keto tautomerism with the enol form being colourless and the keto form being coloured (Hadjoudis *et. al.*,

2004; Robert *et. al.*, 2009). However, it has also been found that temperature-induced fluorescence also plays a significant role in the colour change observed, particularly upon cooling (Harada *et. al.*, 2007). Diffuse reflectance spectra were collected for **1-Br** to **9-Br** and are available in the Supplementary Information Figures S1-S9. No account was taken of the potential effect of fluorescence, however the spectra are presented to support the visually observed trends. In the reflectance spectra for the more strongly thermochromic complexes (**1**, **3**, **4**, **6**, **7** and **9**) the reflectance decreases rapidly below ~580 nm as the temperature is reduced, which is consistent with a lightening in colour. While for the weakly thermochromic compounds (**2**, **5** and **8**) much smaller decreases in reflectance were observed upon cooling below ~490 nm. To look for evidence of proton transfer in two of the crystals showing significant colour changes, **3-Cl** and **3-Br**, variable temperature neutron diffraction was carried out. However, no evidence of the proton shifting was identified and the O-H proton was located at essentially the same position at both 300(2) and 120(2) K for both structures. It is possible that the level of the cis-keto form was too small to be detected crystallographically.

3.6. Structural analysis

A packing similarity tree diagram for the structures, calculated using CSD Materials in Mercury (Macrae *et. al.*, 2008) and allowing for structural variations, highlights both links between structures with similar packing and the wide range of packing observed, Figure 10. The point at which structures meet at a node highlights the number of molecules in a cluster around the central molecule that are similar so for example **1-F** and **7-Br** have twelve molecules in common while **1-Cl** and **1-Br** are essentially isostructural with fifteen molecules in common. For completeness the location of the three published structures differing to the structures determined in this study have been included on the diagram. Unsurprisingly for **9-Br** which undergoes a space group change upon cooling (*Pc* to *Cc*) the packing in the room temperature structure (Ozek *et. al.*, 2007) has a very high similarity to the 120(2) K structure. In general, it is worth noting that the structures showing high similarity in their packing with ≥ 12 molecules in common, tend to be pairs or groups that are either moderately/strongly thermochromic or weakly thermochromic. The main exception to this rule is that the weakly thermochromic **8-F** and **8-Br** have very similar structures to **9-Br** which by eye show a larger colour change.

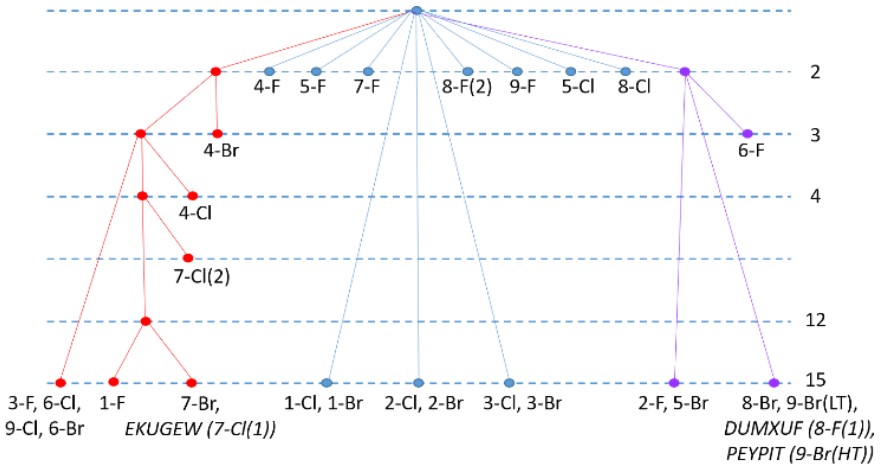

Figure 10 Packing similarity diagram calculated using CSD Materials in Mercury (Macrae *et. al.*, 2008) and allowing for structural variations. Both polymorphs of **8-F** and **7-Cl** are included along with the 300 K (HT) and 120 K (LT) structures of **9-Br**.

The dihedral angles between the two phenyl rings are given in Table 2 and show wide variations from 2.07(9)° in **8-F(2)** to 56.74(7)° in **2-F**. In some Schiff bases a link between the dihedral angle and chromic behaviour has been proposed (Hadjoudis *et. al.*, 2004; Robert *et. al.*, 2009), compounds with $\Phi < 25°$ are expected to be strongly thermochromic due to the higher basicity of the imine nitrogen and as Φ increases the degree of thermochromism is expected to reduce. In the compounds studied here there is some variation from this expected trend with three of the strongly thermochromic compounds **4-F**, **6-F** and **9-Br** having large Φ values of 30.60(8)°, 29.53(4)° and 38.42(16)° respectively, while three of the weakly thermochromic compounds **5-F**, **8-F(2)** and **8-Cl** have very small or small Φ values of 2.40(11)°, 2.07(9)° and 16.33(20)° respectively. No significant correlation between the halogen substituent position and the thermochromic behaviour was identified in this study.

Table 2 Dihedral angles between the two phenyl rings for all of the compounds. Both polymorphs of **7-Cl** and **8-F** are included. Note **7-Cl(2)** has *Z*'=2.

Compound prefix	Halogen position	OMe position	F	Cl	Br
1	2	3	6.19(11)	7.20(10)	6.887(21)
2	2	4	56.754(7)	24.15(5)	23.70(8)
3	2	5	5.66(7)	11.13(7)	13.86(13)
4	3	3	30.60(8)	0.60(11)	24.09(11)
5	3	4	2.40(11)	28.38(5)	42.72(12)
6	3	5	29.523(4)	5.64(15)	5.4331(741)
7	4	3	10.48(5)	**7-Cl(1)**[i] 11.9°	10.8810(3620)
				7-Cl(2) 11.75(11) 16.73(11)	
8	4	4	**8-F(1)**[ii] 48.17(1)	16.2633(210)	48.676(7)
			8-F(2) 2.07(9)		
9	4	5	20.60(4)	7.71(9)	38.42(16)

[i] Yeap *et. al.*, 2003, [ii] Albayrak *et. al.*, 2010

4. Conclusions

The structures of 27 *N*-(methoxysalicylidene)-haloaniline (halo = F, Cl or Br) are reported at 150(2), 120(2) or 100(2) K. Ten of these structures had previously been reported at room temperature and the structures herein were the same. While in the case of **8-F** and **7-Cl** new polymorphs are reported which show significant differences in their packing compared to the previously reported polymorphs. In addition, a phase transition was identified for **9-Br**, which occurs somewhere between 200(2) and 120(2) K. No phase transitions were identified between 300(2) and 120(2) K for any of the other compounds.

The 4-methoxysalicyl derivatives are yellow at room temperature and display very little colour change by eye when dipped in liquid nitrogen, ~77 K, whereas the 3 or 5-methoxysalicyl compounds are orange / red at room temperature and show a dramatic colour change with decreasing temperature down to yellow at liquid nitrogen temperatures. The colour change has previously been associated with the occurrence of a temperature induced enol to *cis*-keto tautomerism with temperature induced fluorescence also having a significant impact. Herein neutron diffraction studies on **3-Cl** and **3-Br** showed no evidence of proton shifting, so it is possible that the level of the *cis*-keto form was too

small to be detected crystallographically but also no investigation was made into the effect of fluorescence on the or the colour change in the complexes.

While both the nature of the packing and the compounds' *inter*planar angle are believed to affect the thermo- and photochromic properties of the anils, the type and position of substituents can also be important. The position of the strongly electron donating methoxy group on the salicyl moiety appears to have a stronger influence on the colour and thermochromic properties of the anils than the location of the weakly electron withdrawing halogen on the aniline moiety. The 3- and 5- methoxy compounds visually showed significant colour changes upon cooling, while the 4-methoxy compounds showed relatively small colour changes. While the majority of the 3- and 5- methoxy compounds had dihedral angles Φ of < 25° there were several exceptions to the rule.

Acknowledgements The authors are grateful to Professor Andrew Beeby, Durham University for help with discussions on the chromism. HEM is grateful to the EPSRC and Durham University for funding and Professor Jonathan Steed, Durham University for useful discussions.

References

Albayrak, C., Ozek, A., Kosar, B., Odabasoglu, M. & Buyukgungor, O. (2010). *Acta Cryst*, **E66**, o315.

Allen, F. H., Kennard, O., Watson, D. G., Brammer, L., Orpen, A. G. & Taylor, R. (1987). *J. Chem. Soc., Perkin Trans 2*, S1-S19.

Cohen, M. D. & Schmidt G. M. J. (1962). *J. Phys. Chem.*, **66**, 2442-2446.

Cohen, M. D., Schmidt, G. M. J. & Flavian, S. (1964). *J. Chem. Soc.*, 2041-2051.

D'Oria, E. & Novoa, J. J. (2008). *CrystEngComm*, **10**, 423-436.

Dolomanov, O. V., Bourhis, L. J., Gildea, R. J., Howard, J. A. K. & Puschmann, H. (2009). *J. Appl. Cryst.*, **42**, 339-341.

Francis, S., Muthiah, P. T., Venkatachalam, G. & Ramesh, R. (2003). *Acta Cryst*, **E59**, o1045-o1047.

Fujiwara, T., Harada, J. & Ogawa, K. (2004). *J. Phys. Chem.*, **B108**, 4035-4038.

Gu, Y. L., Kar, T. & Scheiner, S. (1999). *J. Am. Chem. Soc.*, **121**, 9411-9422.

Gutmann, M. J. (2005). SXD2001.

Hadjoudis, E. & Mavridis, I. M. (2004). *Chem. Soc. Revs*, **33**, 579-588.

Harada, J., Uekusa, H. & Ohashi, Y. (1999). *J. Am. Chem. Soc.*, **121**, 5809-5810.

Harada, J., Fujiwara, T. & Ogawa, K. (2007). *J. Am. Chem. Soc.*, **129**, 16216-16221.

Kargar, H., Torabi, V., Akbari, A., Behjatmanesh-Ardakani, R., Sahraei, A. & Tahir, M. N. (2020). *J. Mol. Struct.*, 1205.

Keen, D. A., Gutmann, M. J. & Wilson, C. C. (2006). *J. Appl. Cryst.*, **39**, 714-722.

Kosar, B., Albayrak, C., Odabasoglu, M. & Buyukgungor, O.(2009). *Acta Cryst.*, **C65**, o517-o520.

Kumari, S., Das, B. & Ray, S. (2019). *Dalton Transactions*, **48**, 15942-15954.

Macrae, C. F., Bruno, I. J., Chisholm, J. A., Edgington, P. R., McCabe, P., Pidcock, E., Rodriguez-Monge, L., Taylor, R., van de Streek, J. & Wood, P. A. (2008). *J. Appl. Cryst*, **41**, 466-470.

Mighani, H. (2020). *Journal of Polymer Research*, 27.

Ogawa, K., Kasahara, Y., Ohtani, Y. & Harada, J. (1998). *J. Am. Chem. Soc.*, **120**, 7107-7108.

Ogawa, K., Harada, J., Tamura, I. & Noda, Y. (2000). *Chemistry Letters*, 528-529.

Ozek, A., Albayrak, C., Odabasoglu, M. & Buyukgungor, O. (2007). *Acta Cryst*, **C63**, o177-o180.

Ozek, A., Buyukgungor, O., Albayrak, C. & Odabasoglu, M. (2008a). *Acta Cryst*, **E64**, o1579-o1580.

Özek, A., Albayrak, Ç., Odabaşoğlu, M. & Büyükgüngör, O. (2008b). *J. Chem. Cryst.*, **39**, 353-357.

Ozek, A., Buyukgungor, O., Albayrak, C. & Odabasoglu, M. (2008c). *Acta Cryst*, E64, o1613-o1614.

Palatinus, L. & Chapuis, G. (2007). *J. Appl. Cryst.*, **40**, 786-790.

Palatinus, L. & van der Lee, A. (2008). *J. Appl. Cryst.*, **41**, 975-984.

Palatinus, L., Prathapa, S. J. & van Smaalen, S. (2012). *J. Appl. Cryst.*, **45**, 575-580.

Parveen, S. (2020). *Applied Organometallic Chemistry*, https://doi.org/10.1002/aoc.5687

Robert, F., Naik, A. D., Tinant, B., Robiette, R. & Garcia, Y. (2009). *Chemistry-a European Journal*, **15**, 4327-4342.

Sahu, M., Manna, A. K., Rout, K., Mondal, J. & Patra, G. K. (2020). *Inorganica Chimica Acta*, 508.

Senier, A. & Shepheard, F. G. (1909). *J. Chem. Soc., Trans.*, **95**, 1943-1955.

Sheldrick, G. M. (2008). *Acta Cryst*., **A64**, 112-122.

Sheldrick, G. M. (2015). *Acta Cryst*.. **C71**, 3-8.

Thalladi, V. R., Weiss, H. C., Blaser, D., Boese, R., Nangia, A. & Desiraju, G. R. (1998). *J. Am. Chem. Soc.*, **120**, 8702-8710.

Unver, H., Kendi, E., Guven, K. & Durlu, T. N. (2002). *Zeitschrift Fur Naturforschung*, **B57**, 685-690.

Yeap, G.-Y., Ha, S.-T., Ishizawa, N., Suda, K., Boey, P.-L. & Kamil Mahmood, W. A. (2003). *J. Mol. Struct.*, **658**, 87-99.

Zheng, C.-S., Yang, N., Li, M. & Jing, Z.-L. (2005). *Acta. Cryst*. **E61**, o3613-o3614.

Supporting information

Table S1 Crystal data and structure refinement for **1-F** to **9-F**.

Identification code	**1-F**	**2-F**	**3-F**	**4-F**	**5-F**	**6-F**	**7-F**	**8-F**	**9-F**
Empirical formula	$C_{14}H_{12}FNO_2$	$C_{14}H_{12}FNO_2$	$C_{14}H_{12}FNO_2$	$C_{14}H_{12}FNO_2$	$C_{14}H_{12}FNO_2$	$C_{14}H_{12}FNO_2$	$C_{14}H_{12}FNO_2$	$C_{14}H_{12}FNO_2$	$C_{14}H_{12}FNO_2$
Formula weight	245.25	245.25	245.25	245.25	245.25	245.25	245.25	245.25	245.25
Temperature/K	120(2)	120(2)	120(2)	120.15	120(2)	120(2)	120(2)	120(2)	120(2)
Crystal system	orthorhombic	orthorhombic	monoclinic	orthorhombic	monoclinic	monoclinic	monoclinic	monoclinic	monoclinic
Space group	$P2_12_12_1$	$Pbca$	$P2_1/c$	$Pna2_1$	$P2_1/c$	$P2_1/c$	$P2_1/c$	$P2_1/c$	$C2/c$
a/Å	5.0834(2)	6.2970(8)	20.3838(10)	19.3411(12)	3.8058(3)	13.1230(9)	11.3352(7)	3.8354(3)	28.1425(12)
b/Å	12.4697(5)	25.465(3)	4.6633(2)	4.9865(3)	10.6818(8)	13.2386(9)	12.0366(7)	10.6493(7)	6.9311(3)
c/Å	18.1059(8)	14.3055(14)	12.6117(6)	12.2219(8)	27.574(2)	6.8116(4)	9.3002(6)	27.9772(19)	12.8535(5)
α/°	90	90	90	90	90	90	90	90	90
β/°	90	90	106.7470(10)	90	91.609(2)	103.690(2)	114.1750(10)	90.8060(10)	113.2170(10)
γ/°	90	90	90	90	90	90	90	90	90
Volume/Å^3	1147.71(8)	2294.0(5)	1147.97(9)	1178.73(13)	1120.53(15)	1149.76(13)	1157.61(12)	1142.60(14)	2304.15(17)
Z	4	8	4	4	4	4	4	4	8
ρ_{calc}g/cm^3	1.419	1.420	1.419	1.382	1.454	1.417	1.407	1.426	1.414
μ/mm^{-1}	0.106	0.106	0.106	0.103	0.109	0.106	0.105	0.107	0.106
F(000)	512.0	1024.0	512.0	512.0	512.0	512.0	512.0	512.0	1024.0
Crystal size/mm^3	0.4 × 0.26 × 0.2	0.41 × 0.28 × 0.03	0.44 × 0.3 × 0.16	0.46 × 0.26 × 0.14	0.2 × 0.16 × 0.06	0.38 × 0.24 × 0.18	0.4 × 0.3 × 0.26	0.46 × 0.14 × 0.12	0.42 × 0.32 × 0.3
Radiation	MoKα (λ = 0.71073)	MoKα (λ = 0.71073)	MoKα (λ = 0.71073)	MoKα (λ = 0.71073)	MoKα (λ = 0.71073)	MoKα (λ = 0.71073)	MoKα (λ = 0.71073)	MoKα (λ = 0.71073)	MoKα (λ = 0.71073)
2θ range for data collection/°	3.966 to 56.55	5.696 to 51.364	4.174 to 56.564	4.212 to 56.564	2.956 to 51.362	3.194 to 51.354	3.938 to 56.564	2.912 to 52.744	3.15 to 56.562
Index ranges	-6 ≤ h ≤ 6, -16 ≤ k ≤ 16, -24 ≤ l ≤ 24	-7 ≤ h ≤ 7, -31 ≤ k ≤ 29, -17 ≤ l ≤ 17	-27 ≤ h ≤ 27, -6 ≤ k ≤ 6, -16 ≤ l ≤ 16	-25 ≤ h ≤ 25, -6 ≤ k ≤ 6, -16 ≤ l ≤ 16	-4 ≤ h ≤ 4, -13 ≤ k ≤ 13, -33 ≤ l ≤ 33	-16 ≤ h ≤ 15, -14 ≤ k ≤ 16, -6 ≤ l ≤ 8	-15 ≤ h ≤ 15, -16 ≤ k ≤ 16, -12 ≤ l ≤ 12	-4 ≤ h ≤ 4, -13 ≤ k ≤ 13, -34 ≤ l ≤ 34	-37 ≤ h ≤ 37, -9 ≤ k ≤ 8, -16 ≤ l ≤ 17
Reflections collected	15619	8769	12140	12283	10327	6467	12782	10926	12612
Independent reflections	2845 [R_{int} = 0.0381, R_{sigma} = 0.0259]	2179 [R_{int} = 0.1099, R_{sigma} = 0.1057]	2834 [R_{int} = 0.0291, R_{sigma} = 0.0238]	2930 [R_{int} = 0.0267, R_{sigma} = 0.0217]	2129 [R_{int} = 0.0653, R_{sigma} = 0.0519]	2183 [R_{int} = 0.0359, R_{sigma} = 0.1086]	2872 [R_{int} = 0.0891, R_{sigma} = 0.0525]	2336 [R_{int} = 0.0443, R_{sigma} = 0.0354]	2865 [R_{int} = 0.0333, R_{sigma} = 0.0259]
Data/restraints/parameters	2845/0/168	2179/0/168	2834/0/168	2930/1/168	2129/0/168	2183/0/174	2872/0/168	2336/0/168	2865/0/168
Goodness-of-fit on F^2	1.036	1.110	1.065	1.044	1.025	1.075	1.043	1.035	1.039
Final R indexes [I>=2σ (I)]	R_1 = 0.0337, wR_2 = 0.0835	R_1 = 0.0845, wR_2 = 0.1122	R_1 = 0.0383, wR_2 = 0.0985	R_1 = 0.0302, wR_2 = 0.0747	R_1 = 0.0514, wR_2 = 0.1096	R_1 = 0.0472, wR_2 = 0.1310	R_1 = 0.0445, wR_2 = 0.1136	R_1 = 0.0499, wR_2 = 0.1097	R_1 = 0.0408, wR_2 = 0.1044
Final R indexes [all data]	R_1 = 0.0427, wR_2 = 0.0900	R_1 = 0.1369, wR_2 = 0.1289	R_1 = 0.0499, wR_2 = 0.1043	R_1 = 0.0351, wR_2 = 0.0776	R_1 = 0.0916, wR_2 = 0.1262	R_1 = 0.0708, wR_2 = 0.1486	R_1 = 0.0642, wR_2 = 0.1249	R_1 = 0.0723, wR_2 = 0.1182	R_1 = 0.0553, wR_2 = 0.1130
Largest diff. peak/hole / e Å^{-3}	0.20/-0.16	0.27/-0.28	0.25/-0.21	0.18/-0.18	0.23/-0.21	0.15/-0.24	0.40/-0.20	0.18/-0.22	0.26/-0.18

Table S2 Crystal data and structure refinement for **1-Cl** to **9-Cl**.

Identification code	**1-Cl**	**2-Cl**	**3-Cl**	**4-Cl**	**5-Cl**	**6-Cl**	**7-Cl**	**8-Cl**	**9-Cl**
Empirical formula	$C_{14}H_{12}ClNO_2$	$C_{14}H_{12}ClNO_2$	$C_{14}H_{12}ClNO_2$	$C_{14}H_{12}ClNO_2$	$C_{14}H_{12}ClNO_2$	$C_{14}H_{12}ClNO_2$	$C_{14}H_{12}NO_2Cl$	$C_{14}H_{12}NO_2Cl$	$C_{14}H_{12}NO_2Cl$
Formula weight	261.70	261.70	261.70	261.70	261.70	261.70	261.70	261.70	261.70
Temperature/K	120(2)	120(2)	120(2)	100(2)	150(2)	100(2)	120(2)	120(2)	120(2)
Crystal system	orthorhombic	monoclinic	monoclinic	orthorhombic	monoclinic	monoclinic	monoclinic	monoclinic	monoclinic
Space group	*Pna*2$_1$	*C*2/*c*	*P*2$_1$/*c*	*P*2$_1$2$_1$2$_1$	*C*2/*c*	*Pc*	*P*2$_1$/*c*	*P*2$_1$/*c*	*P*2$_1$/*c*
a/Å	6.4045(2)	22.2996(14)	13.1915(3)	4.9119(2)	14.1997(4)	12.5233(5)	4.8166(4)	5.5216(11)	21.2023(12)
b/Å	14.5211(4)	7.2002(5)	8.2973(2)	12.4251(5)	6.5840(2)	4.4479(2)	21.3693(16)	8.8865(18)	4.6591(3)
c/Å	12.9892(3)	16.4795(11)	11.9180(2)	19.5142(7)	26.2190(7)	11.8828(6)	23.8639(16)	25.127(5)	12.1240(7)
α/°	90	90	90	90	90	90	90	90	90
β/°	90	113.2315(9)	112.5479(12)	90	102.2648(19)	113.577(3)	92.844(3)	95.001(5)	93.615(2)
γ/°	90	90	90	90	90	90	90	90	90
Volume/Å^3	1208.00(6)	2431.4(3)	1204.76(5)	1190.97(8)	2395.29(12)	606.65(5)	2453.2(3)	1228.2(4)	1195.27(12)
Z	4	8	4	4	8	2	8	4	4
ρ_{calc}g/cm^3	1.439	1.430	1.443	1.460	1.451	1.433	1.417	1.415	1.454
μ/mm^{-1}	0.308	0.306	0.309	0.313	0.311	0.307	0.304	0.303	0.312
F(000)	544.0	1088.0	544.0	544.0	1088.0	272.0	1088.0	544.0	544.0
Crystal size/mm^3	0.44 × 0.28 × 0.19	0.42 × 0.41 × 0.32	0.35 × 0.34 × 0.22	0.25 × 0.2 × 0.15	0.67 × 0.49 × 0.20	0.25 × 0.18 × 0.12	0.48 × 0.28 × 0.08	0.28 × 0.08 × 0.03	0.33 × 0.11 × 0.08
Radiation	MoKα (λ = 0.71073)	MoKα (λ = 0.71073)	MoKα (λ = 0.71073)	MoKα (λ = 0.71073)	MoKα (λ = 0.71073)	MoKα (λ = 0.71073)	MoKα (λ = 0.71073)	MoKα (λ = 0.71073)	MoKα (λ = 0.71073)
2θ range for data collection/°	4.208 to 56.08	3.976 to 56.176	3.342 to 56.134	3.886 to 56.376	3.18 to 56.016	6.88 to 56.01	2.56 to 52.74	3.254 to 50.06	3.85 to 52.744
Index ranges	-7 ≤ h ≤ 8, -19 ≤ k ≤ 19, -17 ≤ l ≤ 17	-29 ≤ h ≤ 29, -9 ≤ k ≤ 5, -21 ≤ l ≤ 21	-17 ≤ h ≤ 14, -10 ≤ k ≤ 10, -14 ≤ l ≤ 15	-6 ≤ h ≤ 6, -15 ≤ k ≤ 16, -25 ≤ l ≤ 25	-16 ≤ h ≤ 18, -8 ≤ k ≤ 8, -34 ≤ l ≤ 34	-15 ≤ h ≤ 16, -5 ≤ k ≤ 5, -15 ≤ l ≤ 11	-5 ≤ h ≤ 6, -26 ≤ k ≤ 26, -29 ≤ l ≤ 29	-6 ≤ h ≤ 6, -10 ≤ k ≤ 10, -29 ≤ l ≤ 29	-26 ≤ h ≤ 23, -5 ≤ k ≤ 5, -15 ≤ l ≤ 15
Reflections collected	15606	10887	10548	10919	10346	5290	24571	11727	7498
Independent reflections	2912 [R_{int} = 0.0289, R_{sigma} = 0.0224]	2956 [R_{int} = 0.0174, R_{sigma} = 0.0162]	2920 [R_{int} = 0.0271, R_{sigma} = 0.0272]	2927 [R_{int} = 0.0315, R_{sigma} = 0.0309]	2895 [R_{int} = 0.0256, R_{sigma} = 0.0248]	2268 [R_{int} = 0.0247, R_{sigma} = 0.0325]	4976 [R_{int} = 0.0512, R_{sigma} = 0.0409]	2175 [R_{int} = 0.0686, R_{sigma} = 0.0574]	2429 [R_{int} = 0.0277, R_{sigma} = 0.0299]
Data/restraints/parameters	2912/1/168	2956/0/168	2920/0/168	2927/0/169	2895/0/168	2268/2/168	4976/0/335	2175/0/168	2429/0/168
Goodness-of-fit on F^2	1.053	1.037	1.045	1.046	1.051	1.049	1.067	1.074	1.076
Final R indexes [I>=2σ (I)]	R_1 = 0.0249, wR_2 = 0.0600	R_1 = 0.0296, wR_2 = 0.0788	R_1 = 0.0292, wR_2 = 0.0754	R_1 = 0.0294, wR_2 = 0.0676	R_1 = 0.0352, wR_2 = 0.0856	R_1 = 0.0298, wR_2 = 0.0680	R_1 = 0.0439, wR_2 = 0.0842	R_1 = 0.0648, wR_2 = 0.1683	R_1 = 0.0379, wR_2 = 0.0985
Final R indexes [all data]	R_1 = 0.0273, wR_2 = 0.0612	R_1 = 0.0343, wR_2 = 0.0823	R_1 = 0.0368, wR_2 = 0.0788	R_1 = 0.0352, wR_2 = 0.0697	R_1 = 0.0477, wR_2 = 0.0916	R_1 = 0.0344, wR_2 = 0.0704	R_1 = 0.0619, wR_2 = 0.0892	R_1 = 0.0872, wR_2 = 0.1846	R_1 = 0.0472, wR_2 = 0.1063
Largest diff. peak/hole / e Å^{-3}	0.21/-0.15	0.31/-0.22	0.32/-0.20	0.22/-0.22	0.32/-0.22	0.23/-0.19	0.25/-0.25	0.56/-0.36	0.33/-0.21

Flack parameter	0.028(17)	-	-	0.26(7)	-	0.13(4)	-	-	-

Table S3 Crystal data and structure refinement for **1-Br** to **9-Br**.

Identification code	**1-Br**	**2-Br**	**3-Br**	**4-Br**	**5-Br**	**6-Br**	**7-Br**	**8-Br**	**9-Br 220 K**	**9-Br 120 K**
Empirical formula	$C_{14}H_{12}NO_2Br$	$C_{14}H_{12}NO_2Br$	$C_{14}H_{12}NO_2Br$	$C_{14}H_{12}NO_2Br$	$C_{14}H_{12}NO_2Br$	$C_{14}H_{12}BrNO_2$	$C_{14}H_{12}BrNO_2$	$C_{14}H_{12}NO_2Br$	$C_{14}H_{12}BrNO_2$	$C_{14}H_{12}NO_2Br$
Formula weight	306.16	306.16	306.16	306.16	306.16	306.16	306.16	306.16	306.16	306.16
Temperature/K	120(2)	120(2)	120(2)	120(2)	120(2)	120(2)	120(2)	120(2)	220(2)	120(2)
Crystal system	orthorhombic	monoclinic	monoclinic	monoclinic	orthorhombic	monoclinic	orthorhombic	orthorhombic	monoclinic	monoclinic
Space group	*Pna*2_1	*C*2/*c*	*P*2_1/*c*	*P*2_1/*c*	*Pca*2_1	*Pc*	*P*$2_12_12_1$	*Pna*2_1	*Pc*	*Cc*
a/Å	6.2974(11)	22.351(3)	13.290(2)	12.538(2)	13.823(4)	12.547(4)	4.8326(10)	6.1895(12)	14.077(3)	27.874(5)
b/Å	14.718(2)	7.3950(11)	8.5162(13)	4.8315(9)	14.140(4)	4.4109(16)	12.544(3)	7.0146(13)	6.8915(15)	6.8640(12)
c/Å	13.367(2)	16.267(3)	11.9068(18)	21.010(4)	6.3118(18)	11.895(4)	20.346(4)	28.557(5)	6.5365(13)	6.4840(12)
α/°	90	90	90	90	90	90	90	90	90	90
β/°	90	112.973(2)	113.514(3)	103.043(3)	90	113.687(5)	90	90	98.320(4)	95.091(4)
γ/°	90	90	90	90	90	90	90	90	90	90
Volume/Å^3	1239.0(4)	2475.4(6)	1235.7(3)	1239.9(4)	1233.7(6)	602.9(4)	1233.4(4)	1239.9(4)	627.5(2)	1235.7(4)
Z	4	8	4	4	4	2	4	4	2	4
ρ_{calc}g/cm^3	1.641	1.643	1.646	1.640	1.648	1.687	1.649	1.640	1.620	1.646
μ/mm^{-1}	3.310	3.314	3.319	3.308	3.324	3.402	3.325	3.308	3.268	3.319
F(000)	616.0	1232.0	616.0	616.0	616.0	308.0	616.0	616.0	308.0	616.0
Crystal size/mm^3	0.26 × 0.18 × 0.07	0.35 × 0.24 × 0.14	0.3 × 0.2 × 0.06	0.45 × 0.13 × 0.1	0.3 × 0.08 × 0.03	0.22 × 0.09 × 0.04	0.32 × 0.06 × 0.02	0.4 × 0.31 × 0.18	0.16 × 0.1 × 0.08	0.16 × 0.1 × 0.08
Radiation	MoKα (λ = 0.71073)	MoKα (λ = 0.71073)	MoKα (λ = 0.71073)	MoKα (λ = 0.71073)	MoKα (λ = 0.71073)	MoKα (λ = 0.71073)	MoKα (λ = 0.71073)	MoKα (λ = 0.71073)	MoKα (λ = 0.71073)	MoKα (λ = 0.71073)
2θ range for data collection/°	4.116 to 56.56	3.958 to 54.192	3.342 to 54.204	3.334 to 54.196	2.88 to 54.166	3.544 to 51.354	3.814 to 51.362	5.706 to 52.734	5.85 to 54.202	2.934 to 52.726
Index ranges	$-8 \le h \le 8$, $-19 \le k \le 15$, $-12 \le l \le 17$	$-28 \le h \le 28$, $-9 \le k \le 9$, $-20 \le l \le 19$	$-17 \le h \le 15$, $-10 \le k \le 7$, $-14 \le l \le 15$	$-16 \le h \le 16$, $-6 \le k \le 6$, $-26 \le l \le 26$	$-17 \le h \le 16$, $-11 \le k \le 18$, $-8 \le l \le 7$	$-15 \le h \le 15$, $-5 \le k \le 5$, $-14 \le l \le 14$	$-5 \le h \le 5$, $-15 \le k \le 15$, $-24 \le l \le 24$	$-7 \le h \le 7$, $-8 \le k \le 8$, $-34 \le l \le 34$	$-13 \le h \le 18$, $-8 \le k \le 8$, $-8 \le l \le 5$	$-19 \le h \le 34$, $-8 \le k \le 8$, $-7 \le l \le 8$
Reflections collected	7921	12177	7467	11740	7073	4965	11274	10666	3788	3511
Independent reflections	2339 [R_{int} = 0.0423, R_{sigma} = 0.0483]	2729 [R_{int} = 0.0349, R_{sigma} = 0.0286]	2717 [R_{int} = 0.0356, R_{sigma} = 0.0418]	2732 [R_{int} = 0.0440, R_{sigma} = 0.0370]	2474 [R_{int} = 0.0567, R_{sigma} = 0.0738]	2292 [R_{int} = 0.0596, R_{sigma} = 0.0872]	2345 [R_{int} = 0.0796, R_{sigma} = 0.0669]	2444 [R_{int} = 0.0283, R_{sigma} = 0.0361]	1818 [R_{int} = 0.0485, R_{sigma} = 0.0791]	1623 [R_{int} = 0.0479, R_{sigma} = 0.0708]
Data/restraints/parameters	2339/1/169	2729/0/168	2717/0/168	2732/0/168	2474/1/166	2292/2/166	2345/0/169	2444/1/169	1818/2/169	1623/2/169
Goodness-of-fit on F^2	1.023	1.030	1.026	1.075	1.008	1.082	1.104	1.089	1.015	1.119
Final R indexes [I>=2σ (I)]	R_1 = 0.0291, wR_2 = 0.0552	R_1 = 0.0250, wR_2 = 0.0543	R_1 = 0.0290, wR_2 = 0.0625	R_1 = 0.0311, wR_2 = 0.0638	R_1 = 0.0382, wR_2 = 0.0720	R_1 = 0.0558, wR_2 = 0.1267	R_1 = 0.0418, wR_2 = 0.0721	R_1 = 0.0188, wR_2 = 0.0422	R_1 = 0.0370, wR_2 = 0.0694	R_1 = 0.0418, wR_2 = 0.0922
Final R indexes [all data]	R_1 = 0.0407, wR_2 = 0.0589	R_1 = 0.0358, wR_2 = 0.0576	R_1 = 0.0412, wR_2 = 0.0669	R_1 = 0.0475, wR_2 = 0.0685	R_1 = 0.0669, wR_2 = 0.0827	R_1 = 0.0670, wR_2 = 0.1327	R_1 = 0.0632, wR_2 = 0.0779	R_1 = 0.0212, wR_2 = 0.0431	R_1 = 0.0642, wR_2 = 0.0781	R_1 = 0.0492, wR_2 = 0.0960
Largest diff. peak/hole / e Å^{-3}	0.35/-0.33	0.36/-0.38	0.36/-0.37	0.45/-0.48	0.52/-0.43	2.10/-1.70	0.48/-0.85	0.31/-0.31	0.43/-0.46	1.00/-0.57

Table S4 C-H···O interactions in **1-F** to **9-F**.

Compound	Interaction	H···O(Å)	C···O (Å)	C-H···O (°)
1-F	C13-H13···O1^{i}	2.494	3.329(3)	147
2-F	C12-H12···O1^{ii}	2.490	3.438(5)	176
	C14-H14···O2^{iii}	2.572	3.405(4)	147
3-F	C1-H1B···O1^{iv}	2.516	3.471(2)	165
	C6-H6···O2^{v}	2.624	3.487(2)	151
4-F	C6-H6···O1^{vi}	2.690	3.470(3)	140
	C8-H8···O1^{vi}	2.665	3.436(2)	139
5-F	C1-H1B···O1^{vii}	2.608	3.490(3)	150
6-F	C1-H1B···O2^{viii}	2.621	3.537(2)	156
	C10-H10···O2^{ix}	2.533	3.383(2)	149
	C12-H12···O1^{x}	2.383	3.310(3)	165
7-F	C13-H13···O1^{xi}	2.486	3.400(2)	161
	C13-H13···O2^{xi}	2.671	3.257(2)	120
	C14-H14···O2^{xi}	2.698	3.282(2)	120
8-F	C1-H1A···O1^{xii}	2.641	3.531(3)	151
9-F	C10-H10···O2^{xiii}	2.605	3.500(2)	157
	C13-H13···O1^{xiv}	2.555	3.432(2)	154

(i) 1-x, -½+y, 3/2-z, (ii) 3/2-x, -½+y, +z, (iii) 1+x, +y, +z, (iv) 1-x, -½+y, 3/2-z, (v) +x, -½-y, ½+z, (vi) 3/2-x, ½+y, ½+z, (vii) –x, -y, 1-z, (viii) –x, 1-y, 1-z, (ix) +x, +y, -1+z, (x) 1+x, +y, +z, (xi) –x, 1-y, -z, (xii) 1-x, 1-y, -z, (xiii) +x, -1+y, +z, (xiv) –½+x, ½-y, -½+z

Table S5 C-H···O interactions in **1-Cl** to **9-Cl**.

Compound	Interaction	H···O(Å)	C···O (Å)	C-H···O (°)
1-Cl	C13-H13···O1^{i}	2.576	3.497 (3)	164
	C13-H13···O2^{i}	2.639	3.379(3)	135
2-Cl	C3-H3···O2^{ii}	2.756	3.705(2)	177
	C5-H5···O1^{iii}	2.710	3.481(2)	139
	C11-H11···O1^{iv}	2.752	3.564(2)	144
3-Cl	C8-H8···O2^{v}	2.520	3.458(1)	169
	C14-H14···O2^{v}	2.628	3.443(1)	144
	C12-H12···O1^{vi}	2.704	3.242(2)	117
4-Cl	C1-H1A···O2^{vii}	2.606	3.445(3)	146
	C13-H13···O1^{viii}	2.596	3.324(3)	135
5-Cl	C1-H1C···O1^{ix}	2.624	3.350(2)	131
6-Cl	C6-H6···O2^{x}	2.712	3.476(3)	138
	C8-H8···O2^{x}	2.476	3.289(3)	144
7-Cl	C6-H6···O3^{xi}	2.718	3.596(3)	154
	C10-H10···O4^{xii}	2.578	3.199(3)	123
	C11-H11···O4^{xii}	2.630	3.220(3)	121
	C25-H25···O1^{xiii}	2.561	3.476(3)	162
8-Cl	C1-H1C···O1^{xiv}	2.653	3.431(5)	137
	C11-H11···O2^{xv}	2.613	3.336(5)	133
9-Cl	C1-H1B···O1^{xvi}	2.485	3.432(2)	162
	C3-H3···O1^{xvii}	2.633	3.449(2)	144
	C6-H6···O2^{xviii}	2.612	3.431(2)	145
	C8-H8···O2^{xviii}	2.567	3.398(2)	146

(i) 2-x, 1-y, -½+z, (ii) 1-x, -y, 1-z, (iii) ½-x, ½+y, ½-z, (iv) ½+x, ½+y, +z, (v) +x, 3/2-y, -½+z, (vi) -1+x, 3/2-y, -½+z, (vii) -1+x, +y, +z, (viii) 1-x, -½+y, ½-z, (ix) ½-x, 3/2-y, 1-z, (x) +x, 1-y, -½+z, (xi) 2-x, 1-y, 1-z, (xii) 1-x, 1-y, 1-z (xiii) 1-x, -½+y, 3/2-z, (xiv) 2-x, 1-y, 1-z, (xv) –x, -½+y, 3/2-z, (xvi) –x, -½+y, ½-z, (xvii) x, -½-y, ½+z, (xviii) x, ½-y, -½+z

Table S6 C-H···O interactions in **1-Br** to **9-Br**.

Compound	Interaction	H···O(Å)	C···O (Å)	C-H···O (°)
1-Br	C13-H13···O1^{i}	2.587	3.498(5)	161
	C13-H13···O2^{i}	2.647	3.413(5)	138
2-Br	C5-H5···O1^{ii}	2.674	3.447(2)	139
3-Br	C8-H8···O2^{iii}	2.517	3.457(3)	170
4-Br	C13-H13···O1^{iv}	2.692	3.219(3)	116
5-Br	C14-H14···O2^{v}	2.611	3.523(7)	161
6-Br	C6-H6···O2^{vi}	2.711	3.326(13)	144
	C8-H8···O2^{vi}	2.508	3.322(13)	144
7-Br	C1-H1A···O2^{vii}	2.654	3.437(9)	137
	C11-H11···O1^{viii}	2.428	3.296(9)	152
8-Br	C1-H1A···O1^{ix}	2.704	3.488(4)	137
9-Br	C10-H10···O2^{x}	2.421	3.247(11)	145

(i) 1-x, 1-y, ½+z, (ii) 3/2-x, -½+y, ½-z, (iii) +x, ½-y, -½+z, (iv) 1-x, 1-y, -z, (v) +x, +y, 1+z, (vi) x, -y, ½+z, (vii) -1+x, +y, +z, (viii) 1-x, ½+y, 3/2-z, (iv) ½+x. ½-y, +z, (x) +x, +y, -1+z

Table S7 C-H···F short contacts in **1-F** to **9-F**.

Compound	Interaction	H···F(Å)	C···F (Å)	C-H···F (°)
1-F	C5-H5···F1^{i}	2.590	3.250(2)	127
2-F	C11-H11···F1^{ii}	2.557	3.500(4)	172
	C5-H5···F1^{iii}	2.583	3.395(4)	144
3-F	C14-H14···F1^{iv}	2.586	3.063(1)	111
4-F	C13-H13···F1^{v}	2.639	3.398(3)	137
5-F	C1-H1C···F1^{vi}	2.460	3.439(3)	177
	C12-H12···F1^{vii}	2.627	3.449(3)	145
6-F	C1-H1C···F1B^{viii}	2.430	3.106(3)	127
Disordered F				
	C14-H14···F1A^{ix}	2.579	3.243(3)	127
7-F	C4-H4···F1^{x}	2.472	3.421(2)	178
8-F	C13-H13···F1^{xi}	2.634	3.310(2)	130
9-F	C4-H4···F1^{xii}	2.612	3.513(2)	159
	C1-H1C···F1B^{xiii}	2.582	3.321(2)	132

(i) 2-x, -½+y, 3/2-z, (ii) 1-x, 1-y, 1-z, (iii) ½+x, 3/2-y, 1-z, (iv) +x, ½-y, ½+z, (v) 1-x, 3-y, ½+z, (vi) –x, ½+y, ½-z, (vii) 1-x, -y, -z, (viii) -1+x, +y, -1+z, (ix) +x, +y, 1+z, (x) 1+x, 3/2-y, 3/2+z , (xi) 2-x, 1-y, 1-z, (xii) ½+x, ½-y, ½+z, (xiii) ½+x, -½-y, ½+z.

Table S8 π-π interactions identified within the 27 compounds studied.

Compound	Plane 1	Plane 2	Centroid-centroid distance (Å)	Shift distance (Å)
5-F	C2-C7	C2-C7^{i}	3.806	1.626
	C9-C14	C9-C14^{i}	3.806	1.699
6-F	C2-C7	C2-C7^{ii}	3.804	1.537
	C9-C14	C9-C14^{iii}	3.957	1.996
8-F	C2-C7	C2-C7^{i}	3.835	1.683
	C9-C14	C9-C14^{i}	3.835	1.658
1-Cl	C2-C7	C9-C14^{iv}	3.641	1.263
3-Cl	C2-C7	C2-C7^{iii}	3.825	1.789
5-Cl	C2-C7	C9-C14^{v}	3.750	1.339
1-Br	C2-C7	C9-C14^{iv}	3.672	1.471
3-Br	C2-C7	C2-C7^{vi}	3.808	1.676
5-Br	C2-C7	C9-C14^{vii}	3.867	1.314

(i) -1+x, +y, +z and 1+x, +y, +z, (ii) –x, 1-y, 1-z, (iii) 1-x, 1-y, 1-z, (iv) -1+x, +y, +z, (v) 1-x, +y, ½-z, (vi) 2-x, -y, 1-z, (vii) 1-x, 1-y, -½+z

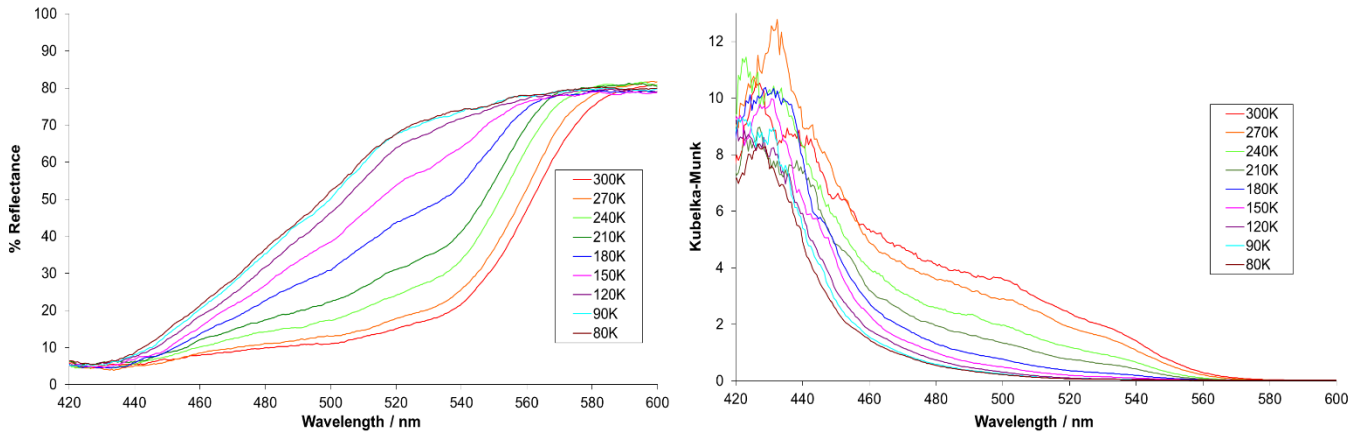

Figure S1 Variable temperature diffuse reflectance spectra between 300 and 80K for **1-Br**, illustrated as wavelength versus (left) % reflectance and (right) the Kubelka-Munk function.

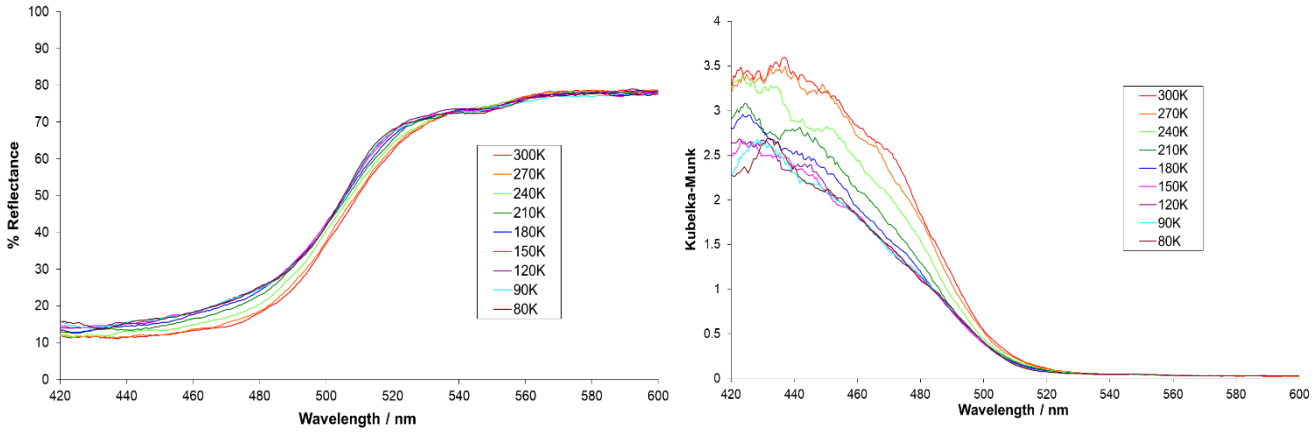

Figure S2 Variable temperature diffuse reflectance spectra between 300 and 80K for **2-Br**, illustrated as wavelength versus (left) % reflectance and (right) the Kubelka-Munk function.

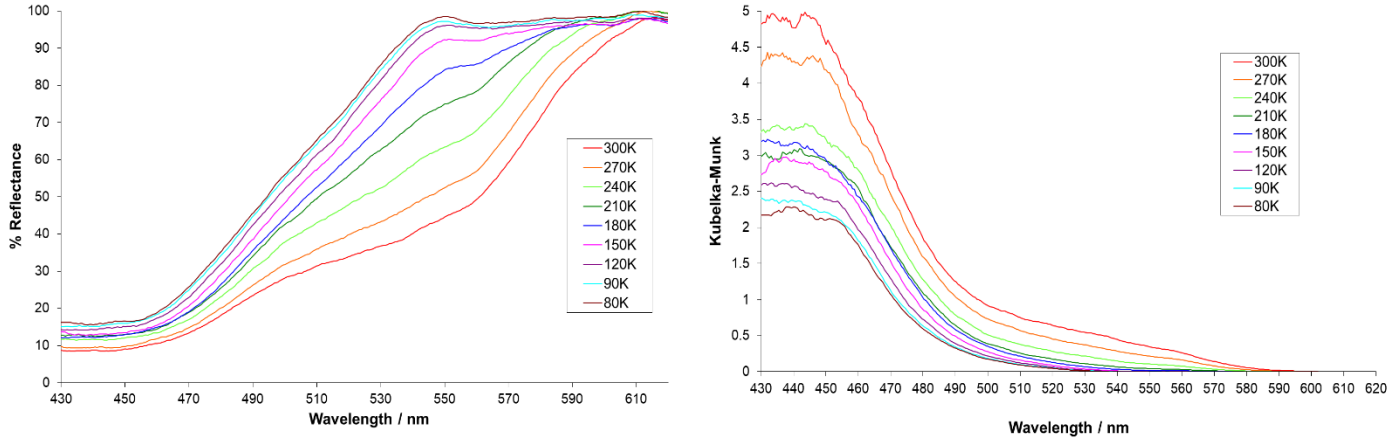

Figure S3 Variable temperature diffuse reflectance spectra between 300 and 80K for **3-Br**, illustrated as wavelength versus (left) % reflectance and (right) the Kubelka-Munk function.

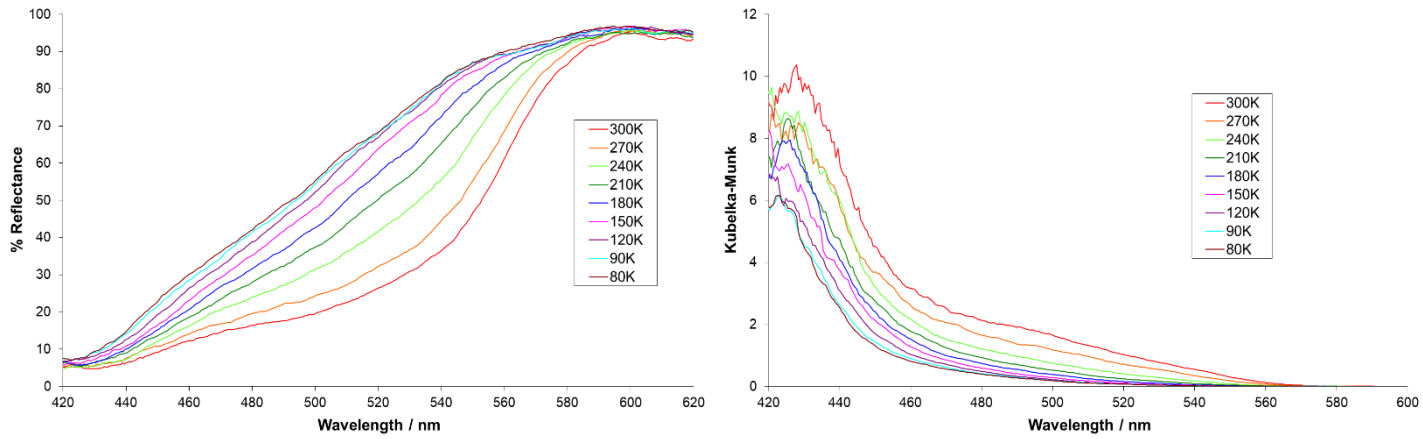

Figure S4 Variable temperature diffuse reflectance spectra between 300 and 80K for **4-Br**, illustrated as wavelength versus (left) % reflectance and (right) the Kubelka-Munk function.

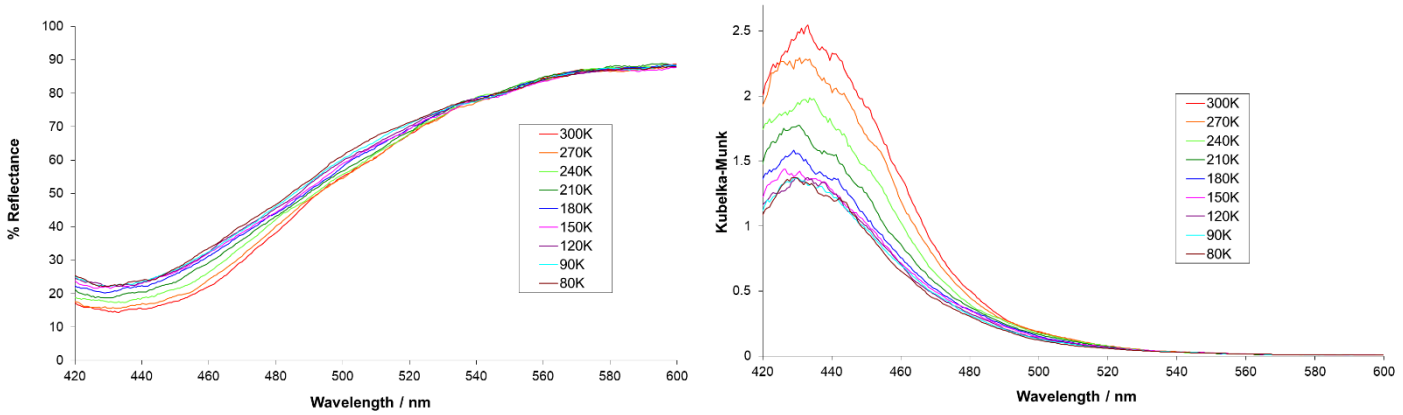

Figure S5 Variable temperature diffuse reflectance spectra between 300 and 80K for **5-Br**, illustrated as wavelength versus (left) % reflectance and (right) the Kubelka-Munk function.

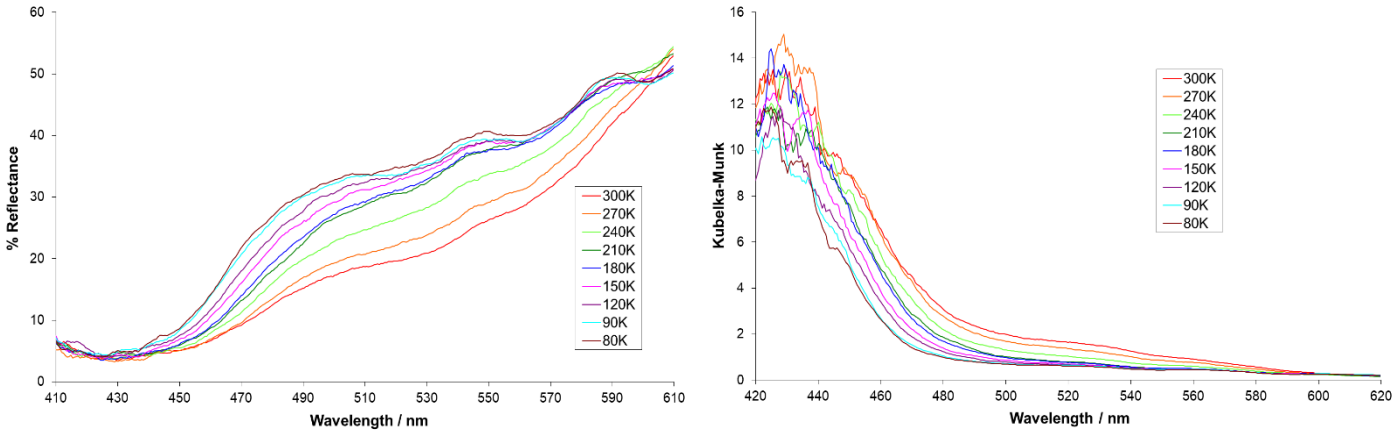

Figure S6 Variable temperature diffuse reflectance spectra between 300 and 80K for **6-Br**, illustrated as wavelength versus (left) % reflectance and (right) the Kubelka-Munk function.

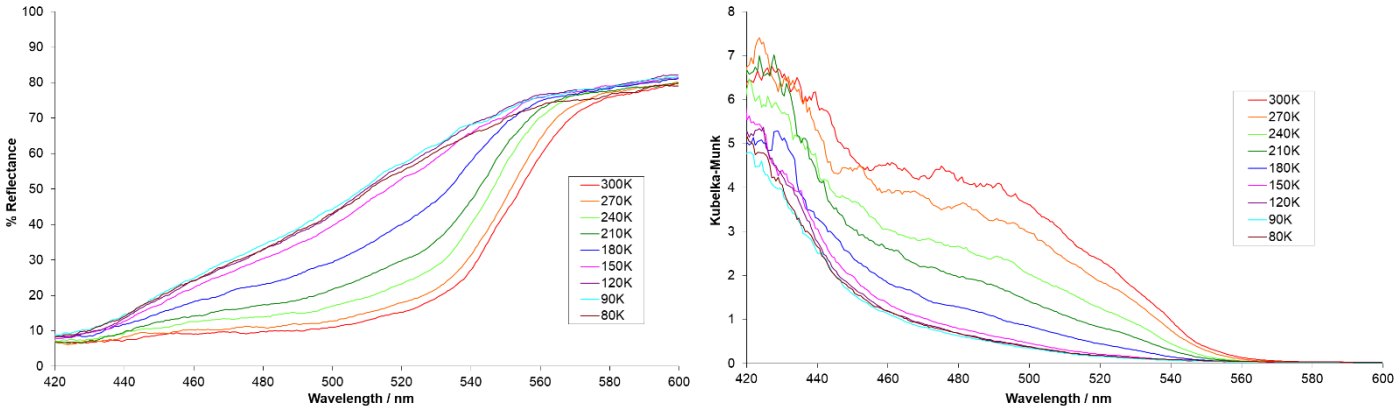

Figure S7 Variable temperature diffuse reflectance spectra between 300 and 80K for **7-Br**, illustrated as wavelength versus (left) % reflectance and (right) the Kubelka-Munk function.

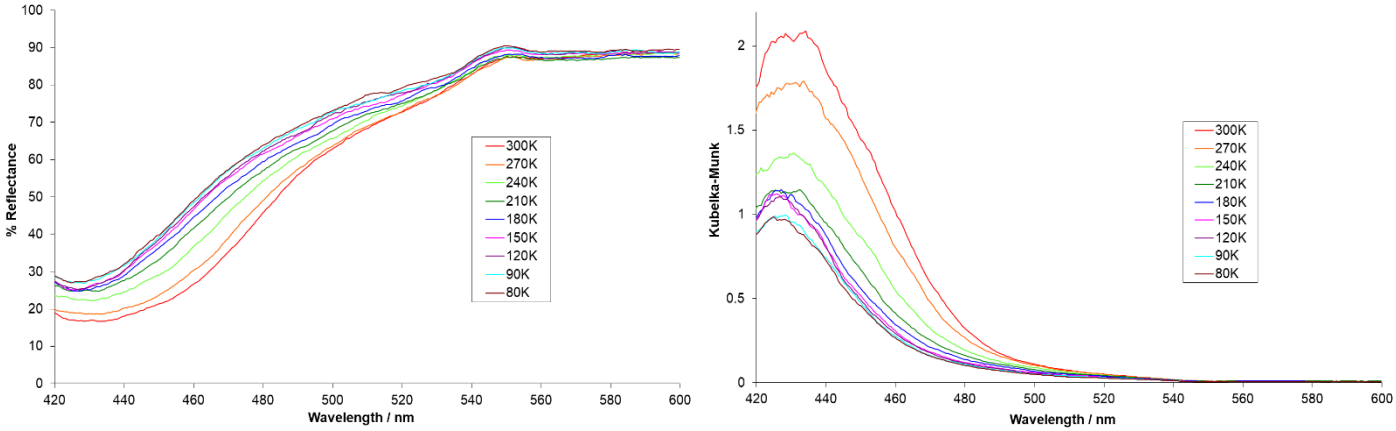

Figure S8 Variable temperature diffuse reflectance spectra between 300 and 80K for **8-Br**, illustrated as wavelength versus (left) % reflectance and (right) the Kubelka-Munk function.

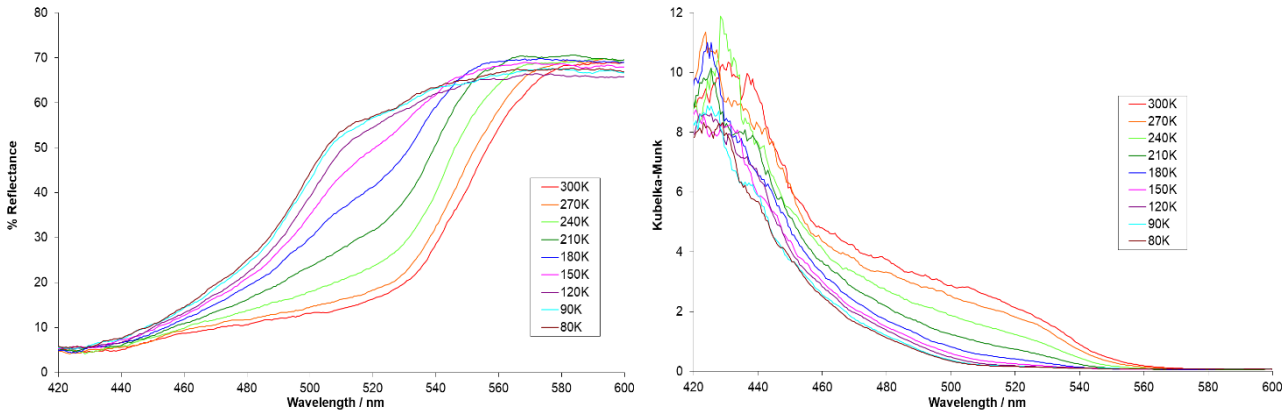

Figure S9 Variable temperature diffuse reflectance spectra between 300 and 80K for **9-Br**, illustrated as wavelength versus (left) % reflectance and (right) the Kubelka-Munk function.